Molecular inheritance from cloud to disk: a story of complex organics and accretion shocks

Gelder, M.L. van

Chapter 1

Introduction

Throughout the entire history of the human race, we have looked up at the sky at night and wondered what those blinking distant lights are. Even far before we knew their precise origin, we connected them into constellations and even used them to navigate ourselves. By looking at the night sky over long periods of time, the by then only known planets Venus, Mars, Jupiter, and Saturn could already be easily distinguished from the more "stationary" light sources.

Initially, the Earth was the center of the universe and everything else was thought to resolve around it, until Copernicus realized that it is the Sun that is the center of our Solar System and that all the planets revolve around the Sun (Copernicus 1543). Later, Galileo Galilei was the first to observe moons around another planet than our own Earth (around Jupiter; Galilei 1610). Over the following centuries, more and more became known about our own Solar System, but several questions remain unanswered. How did the Sun, our Earth, and all the other planets, moons, and comets in our Solar System form? How do all the other stars in our Galaxy form? Are there also planets around other stars? Are we alone?

Especially in the past century, with the level of technology increasing, telescopes have revealed a larger variety of astronomical objects. What were thought to be light dots in the sky, turned out to be distant stars, galaxies, planets, and much more. In addition, also various dark cloud-like areas were discovered (e.g., Barnard 1919; Bok & Reilly 1947). These dark areas, now better known to be molecular clouds, can be as large as hundreds of light-years across. Deep within these cold and dark molecular clouds are the stellar nurseries where new stars are born. So in order to answer the questions related to the formation of our own Solar System, we have to zoom in on the young stellar objects residing deeply within these molecular clouds.

This thesis focuses on how molecules are transported from cloud to disk in the youngest star-forming systems. Observations done with advanced telescopes such as the Atacama Large Millimeter/submillimeter Array (ALMA) are presented

which allow us to study the complex chemistry occurring in these young protostars and their surrounding dark and cold molecular clouds. Furthermore, shock modeling results are presented on whether the material that forms planets is inherited unchanged from the parent molecular cloud or whether it is modified en route.

1.1 How do stars form?

1.1.1 Prestellar phases and start of collapse

Stars are born in dense ($n \sim 10^4 - 10^6$ cm^{-3}) and cold ($T \sim 10 - 20$ K) molecular clouds (see e.g., review by Bergin & Tafalla 2007). These clouds consist mostly of molecular hydrogen (H_2) with carbon monoxide (CO), the next most abundant molecule, being 10 000 times less abundant (Frerking et al. 1982; Lacy et al. 1994, 2017). About 1% of the total mass budget consists of small (sub)micron sized dust grains containing most of the abundant refractory heavy metals such as iron, silicon, and magnesium as well as a significant amount of carbon and oxygen (e.g., Draine & Lee 1984; Henning & Salama 1998; Whittet 2010). However, albeit making up only a small portion of the mass, these dust grains prove to be crucial as a catalyst for the chemistry taking place in these very cold environments (see Sect. 1.2.1).

Molecular clouds can be found throughout the entire Galaxy. Their sizes can vary from being much less than a parsec across (e.g., Bok globules; Bok & Reilly 1947) that will likely form single isolated stars to giant molecular clouds of up to 100 pc across that will likely form clusters of stars (Lada & Lada 2003; Ward-Thompson et al. 2007; Krumholz et al. 2014). Moreover, the total mass of a molecular cloud is also crucial in determining the mass of stars. Molecular clouds are often depicted in schematics as being large spherical clouds but observations in fact show that clouds are far from spherical and can show various possible shapes ranging from small irregular clouds to long filamentary structures (e.g., André et al. 2010; Hacar & Tafalla 2011; Hacar et al. 2013, 2017).

As molecular clouds evolve, the cores within them start to get denser and colder, making them unstable against collapse under their own gravity. At some point, whether it is due to an internal instability or an external trigger, dense cores within molecular clouds will start to collapse. For this, the Jeans criterion should be met (Jeans 1928), that is, that the internal pressure of the core can no longer resist gravity. As the core starts collapsing, the density in the center increases whilst the temperature remains constant. As the inner core becomes optically thick to radiation, it can no longer effectively radiate away the gravitational energy and the temperature of the core increases. The contraction of the core stops, leading to the formation of the First Hydrostatic Core (FHSC; Larson 1969). The temperature in the core keeps increasing until it reaches the threshold where H_2 dissociates (~ 2000 K) that cools down the core. Subsequently, the core contracts further to form a protostar.

In the following two sections, a distinction is made between the next stages of protostellar evolution based on the mass. Low-mass stars ($M < 8$ M$_\odot$) form

significantly slower (up to 10 Myr, see Sect. 1.1.2), whereas high-mass ($M > 8\,\mathrm{M}_\odot$) star formation is much quicker ($10^4 - 10^5$ years, see Sect. 1.1.3) leading to various crucial differences in the evolution of their protostellar phases.

1.1.2 Low-mass star formation

In the process of low-mass star formation, a clear distinction has to be made between evolutionary *Stages* (Shu et al. 1987; Robitaille et al. 2006) and observational *Classes* (Lada 1987; André et al. 1993). As a young protostar is formed, the subsequent evolution can be divided into four stages (see Fig. 1.1). In the first ∼100 000 years, the mass of the system is still dominated by the mass of the envelope (i.e., $M_\mathrm{env} > M_\star$, Stage 0) and the accretion rate onto the protostar is high ($\dot{M} > 10^{-6}$ $\mathrm{M}_\odot$/yr). It is also in this stage that an accretion disk consisting of both gas and dust starts forming around the young protostar to conserve the angular momentum of the rotating core (Cassen & Moosman 1981; Shu et al. 1987). Simulations show that the collapse of a rotating core naturally leads to disks of $10 - 100$ au (e.g., Yorke et al. 1993), although the role of magnetic fields seems crucial in determining the size of the disk through magnetic breaking (e.g., Mellon & Li 2008; Li et al. 2014; Hennebelle et al. 2016). Any excess of angular momentum is removed from the system through bipolar jets and outflows. As the protostar accretes significant amounts of gas, its mass starts exceeding that remaining in the envelope (i.e., $M_\star > M_\mathrm{env} > M_\mathrm{disk}$, Stage 1). Over the next few hundred thousands of years, the protostar keeps accreting mass at a high rate ($\dot{M} > 10^{-6}$ $\mathrm{M}_\odot$/yr) from the disk whereas the envelope accretes onto the disk. Together, Stages 0 and 1 last about ∼500 000 years (Kristensen & Dunham 2018) and are commonly referred to as the *embedded phase of star formation*. The envelope dissipates due to accretion onto the disk and due to the outflow carving a cavity. What remains is a now-called pre-main sequence star which has accreted most of its final mass surrounded by a protoplanetary disk (i.e., $M_\star > M_\mathrm{disk} > M_\mathrm{env}$, Stage 2). The system now slowly evolves over the next $\sim 1 - 5$ million years, where the disk surrounding the pre-main sequence star dissipates through accretion onto the central star (at a much lower rate than in the embedded phase; $\dot{M} < 10^{-6}$ $\mathrm{M}_\odot$/yr), planet formation, and other processes such as photoevaporation. In the final phase (i.e., $M_\star \gg M_\mathrm{disk} \gg M_\mathrm{env}$, Stage 3), a pre-main sequence star remains that evolves toward the main sequence and which is surrounded by a gas-poor debris disk and (presumably) a young planetary system. Finally, the star reaches the main sequence and a young stellar system is born.

Observationally, these various stages are not always trivial to distinguish since the main parameters such as the age of the system, the mass, and accretion rates are not always directly observable. Therefore, these young protostellar systems are generally divided into various Classes based on their spectral energy distribution (SED) at infrared wavelengths (Lada 1987),

$$\alpha_\mathrm{IR} = \frac{d \log \lambda \mathcal{F}_\lambda}{d \log \lambda}, \tag{1.1}$$

where α_IR is the so-called spectral index and $\mathcal{F}_\lambda$ is the observed flux in a wavelength

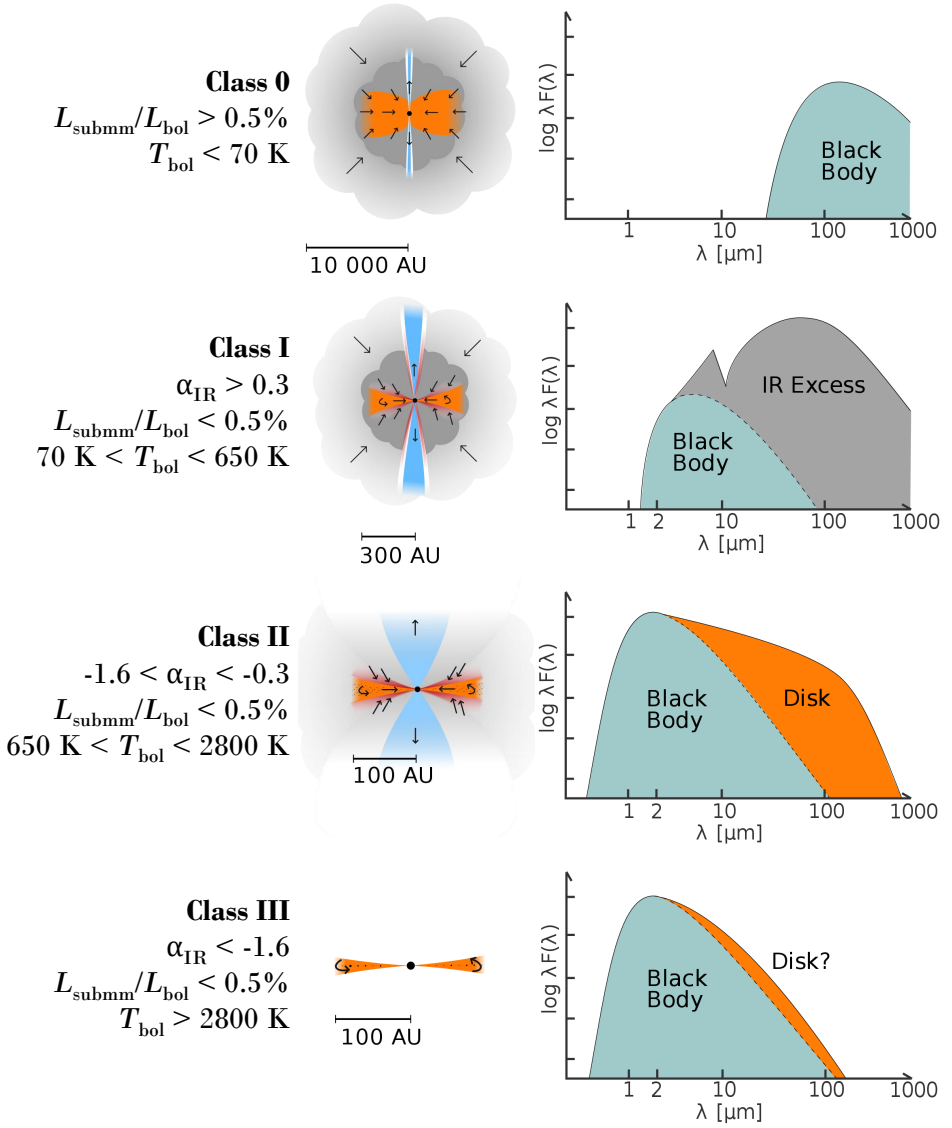

Figure 1.1: Schematic view of the various stages of low-mass star formation. For each observational classification (left), a corresponding schematic of the system (middle) and example SED (right) are presented. Adopted from figure by Magnus Persson.

range of $\lambda = 2 - 20$ μm. Initially, only three Classes were distinguished at infrared wavelengths (I, II, III; Lada 1987), but later different Classes were added such as Class 0 (sources which are too faint at IR wavelengths; André et al. 1993) and Flat-spectrum sources (Greene et al. 1994). Beside using α_{IR} for the classification of protostellar systems, also the bolometric temperature (T_{bol}) and the ratio between

the submillimeter luminosity and bolometric luminosity ($L_{\rm submm}/L_{\rm bol}$) can be used to classify protostellar systems (e.g., André et al. 1993; Chen et al. 1995). Generally, the evolutionary Stages and observational Classes match very well (i.e., a Class I protostar being in Stage I of its evolution). However, it is important to note that the observational parameters depend on the orientation of the source and therefore can mismatch theoretical stages (e.g., Crapsi et al. 2008).

Class 0 protostars are (nearly) invisible at near and mid-infrared wavelengths and are therefore not characterized by $\alpha_{\rm IR}$. Instead, Class 0 protostars are distinguished from more evolved Class I sources through a high $L_{\rm submm}/L_{\rm bol}$ ($> 0.5\%$) and low $T_{\rm bol}$ (< 70 K) (André et al. 1993). Despite strong observational contamination from the envelope, accretion disks are generally still relatively small in Class 0 systems (< 50 au; Tobin et al. 2016; Segura-Cox et al. 2018; Maury et al. 2019), but also large disks have been detected (up to ~ 200 au; Tobin et al. 2012; Murillo et al. 2013). Moreover, molecular jets and outflows that carry away excess angular momentum are most powerful in these young systems (see e.g., reviews by Frank et al. 2014; Bally 2016). Class 0 sources are also the warmest (van 't Hoff et al. 2020c) and most rich in molecular chemistry in their central hot cores (see e.g., review by Jørgensen et al. 2020).

More evolved Class I sources can be distinguished from Class 0 systems by having a high and detectable $\alpha_{\rm IR}$ (> 0.3), lower $L_{\rm submm}/L_{\rm bol}$ ($< 0.5\%$), and higher $T_{\rm bol}$ (70-650 K). The disk mass reservoir in Class I sources is more significant relative to that in the envelope (Jørgensen et al. 2009), and more recently it was suggested that planet formation may start already in these embedded disks based on results on both mass and substructures in the disk (e.g., ALMA Partnership et al. 2015; Tychoniec et al. 2020; Segura-Cox et al. 2020). The bipolar outflows become weaker and more atomic in composition (Arce & Sargent 2006; Nisini et al. 2015). Furthermore, due to the presence of the disk and lower accretion rates, the overall temperature in the systems is lower than in Class 0 sources (van 't Hoff et al. 2018a, 2020b). An exception is in sources where a recent accretion burst has heated the system (van 't Hoff et al. 2018b; Lee et al. 2019b). Flat spectrum sources ($-0.3 < \alpha_{\rm IR} < 0.3$) are suggested to be in an intermediate state between Class I and Class II sources (Greene et al. 1994).

Class II sources are generally also referred to as *T-Tauri stars*, named after the first identified example of a Class II source, and host a *protoplanetary disk* which often show detailed substructures (e.g., Andrews et al. 2018). Since the surrounding envelope has largely dissipated, the photosphere of the central pre-main sequence star can be detected at optical and near-infrared wavelengths as well as an infrared excess originating from the disk at longer wavelengths ($-1.6 < \alpha_{\rm IR} < -0.3$) and a high bolometric temperature ($650 < T_{\rm bol} < 2800$). At this stage, any jet is composed of mostly atomic and ionized material (e.g., Podio et al. 2011; Xie et al. 2021).

Class III sources have only a *debris disk* left containing residual dust that was not accreted onto planetesimals or planets and therefore have only minor infrared excess ($\alpha_{\rm IR} < -1.6$) and high bolometric temperature ($T_{\rm bol} > 2800$ K). These sources show mostly emission originating from the pre-main sequence star that is contracting until hydrogen fusion begins in the core.

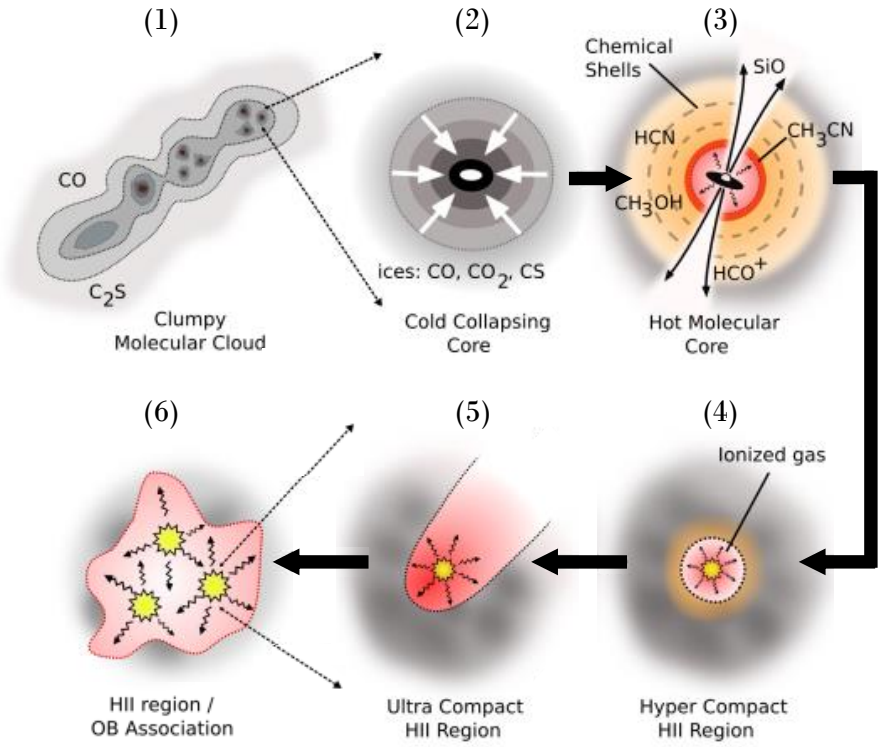

Figure 1.2: Schematic view of the various stages of high-mass star formation. Panels 2-5 are a zoomed in with respect to panel 1 and similarly panel 6 is a zoom-in of panels 2-5. Adopted from figure by Cormac Purcell.

1.1.3 High-mass star formation

In contrast to low-mass stars, high-mass stars are much more difficult to find. Because they are located on the upper end of the initial mass function (Salpeter 1955), they are much rarer than low-mass stars. However, despite being much rarer, high-mass stars are crucial for the evolution of molecular clouds due to their high ionizing radiation and their fate to end in supernova explosions, thereby also triggering sequential star formation. Moreover, high-mass stars form almost exclusively in multiple systems (e.g., Sana et al. 2012).

The formation of massive stars also occurs in a different way from their lower mass counterparts, see Fig. 1.2. High-mass stars form much faster ($\sim$ 0.1 Myr; Beuther et al. 2007) compared to lower mass stars ($\sim 1-5$ Myr), but overall high-mass star formation still remains poorly understood (see reviews by Beuther et al. 2007; Zinnecker & Yorke 2007; Tan et al. 2014; Motte et al. 2018). Starting from a giant molecular cloud, a protostar is formed through collapse in a similar manner as low-mass evolution (Sect 1.1.2). However, due to the large mass of the system, the *hot core* around the center reaches a temperature of $\sim$ 100 K very early,

leading to very rich molecular chemistry (see also Sects 1.2.2 and 1.4.2). As the central protostar increases in mass and approaches the main sequence (whilst still being embedded in its natal envelope), it starts to produce significant amounts of ultraviolet (UV) radiation leading to the formation of an hyper compact HII region (Keto 2003). At this stage, a disk around the high-mass protostar is still likely present (see Beltrán & de Wit 2016, for a review). As the HII region grows into an ultra compact HII region (Churchwell 2002), accretion onto the central massive protostar likely only occurs through the massive disk (e.g., Keto 2007; Kuiper & Hosokawa 2018). Eventually, the radiation pressure disperses the disk completely and accretion halts, leaving a massive star surrounded by a classical HII region.

There are three main theories on how high-mass cores can acquire their mass from the large molecular clouds. In the *monolithic collapse* theory, high-mass star formation is basically a scaled-up version of low-mass star formation where a single cloud or core collapses into a single high-mass protostar (e.g., McKee & Tan 2002). In the *competitive accretion* scenario, high-mass protostars start off as low-mass cores but over time accrete significant amounts of mass from the surrounding molecular cloud (e.g., Bonnell et al. 2001; Bonnell & Bate 2006). Lastly, in the *stellar merger* theory, high-mass stars are suggested to form through mergers of multiple low-mass cores (Bonnell et al. 1998). In reality, all three cases may contribute to the formation of high-mass stars, although stellar mergers seem the least likely process due to the high density of protostellar cores required for stellar mergers to occur.

1.2 Chemistry during protostellar evolution

Atoms and molecules can be used as tracers of various aspects of protostellar evolution. In the local interstellar medium (ISM), the material is largely composed of hydrogen (90%) and helium (10%), with more heavier elements such as carbon (3×10^{-4}), oxygen (4×10^{-4}) and nitrogen (7.5×10^{-5}) occurring in far lower abundances (Wilson & Rood 1994). Furthermore, the metals of which dust grains are composed, such as silicon and iron, are present at even lower levels of $\lesssim 3 \times 10^{-5}$. Yet, despite these lower occurrences, these elements provide the crucial building blocks for the chemistry during the star-formation process, leading to the formation of simple molecules like water (H_2O), methane (CH_4), and ammonia (NH_3), as well as so-called *complex organic molecules* (COMs, molecules containing six or more atoms; Herbst & van Dishoeck 2009) such as methanol (CH_3OH), methyl formate (CH_3OCHO), and ethanol (C_2H_5OH). In total, 241 molecules have been detected in the ISM by mid 2021 (McGuire 2022). It is crucial to understand the relevant chemistry in order to understand why certain molecules trace certain regions in space (Tychoniec et al. 2021).

1.2.1 Prestellar cores

The chemistry in cold and dark prestellar cores is regulated by the low temperatures (< 15 K) and high densities (compared to the general ISM) of $10^4 - 10^6$ cm^{-3}.

At these very low temperatures, the chemistry in the gas phase is dominated by exothermic barrierless reactions, mostly between ions and neutral species or between ions and electrons. The dominant ion in dark cores is H_3^+, which originates from the impact of cosmic rays on H_2. The H_3^+ ion can subsequently react with atoms such as C, O, and N, as well as molecules, leading to the attachment of hydrogen to these species. This eventually leads to the formation of simple molecules such as CO but also longer (and mostly unsaturated) carbon chains (e.g., Langer et al. 1997; Cernicharo et al. 2021, 2022).

Deuterium chemistry

A process that does benefit from the low temperatures in cold and dark clouds is deuterium (D) enhancement (see e.g., reviews by Tielens 2013; Ceccarelli et al. 2014). The canonical D/H fraction in the local ISM is observed to be $2.0\pm0.1\times10^{-5}$ (Linsky et al. 2006; Prodanović et al. 2010). However, the atomic D/H ratio in the gas phase can be increased through the exothermic reaction (Watson 1974),

$$H_3^+ + HD \rightleftharpoons H_2D^+ + H_2 + 232\ \mathrm{K}. \tag{1.2}$$

Since the backward reaction is endothermic, it is less likely to occur at temperatures below $\lesssim 30$ K. H_2D^+ can then subsequently recombine with a free electron to form H_2 and atomic D or transfer its deuterium to other species. It is important to note that Reaction (1.2) can also occur sequentially, leading to the formation D_2H^+ and D_3^+. Moreover, the effectiveness of Reaction (1.2) is enhanced in the densest ($\gtrsim 10^5$ cm^{-3}) regions of the core where CO is frozen out onto the dust grains since CO is the main destroyer of H_3^+ in the gas phase (Brown & Millar 1989; Roberts et al. 2003). Although Reaction 1.2 dominates the deuteration at low temperatures, at higher temperatures deuteration occurs mostly via CH_2D^+ which forms in a similar manner as H_2D^+ but with a higher activation energy barrier for the backward reaction (370 K; Roberts & Millar 2000)

Indeed high H_2D^+/H_3^+ ratios are observed toward the densest parts of prestellar cores (e.g., Caselli et al. 2003, 2008) and the outer parts of protostellar envelopes (Stark et al. 1999). The enhancement of H_2D^+ and CH_2D^+ directly translates into other species in the gas phase such as N_2D^+, DCO^+, DCN, and HDCO (e.g., Roberts et al. 2002; Crapsi et al. 2005). Moreover, species forming through hydrogenation on the surfaces of dust grains can inherit the high atomic D/H ratio leading to deuteration levels as high as a few % for molecules forming on the surfaces of grains (e.g., CH_3OH; van Dishoeck et al. 1995; Bianchi et al. 2017a,b, see also Chapter 4). Due to the sensitivity of Reaction 1.2 to temperature (and density), the deuteration of molecules forming predominantly in the dense prestellar phases can thus be used as a measure of the physical conditions during their formation (e.g., Bøgelund et al. 2018; Taquet et al. 2019).

Grain-surface chemistry

Dust grains make up about 1% of the total mass of molecular clouds and consist mostly of silicates, iron-oxides and carbonaceous material. Yet, they are crucial

for the formation of a large variety of molecules (e.g., Charnley et al. 1992). Atoms such as carbon and nitrogen can stick to the dust grains and be hydrogenated by H-atoms diffusing over the surface (see reviews by van Dishoeck et al. 2013; Tielens 2013; Linnartz et al. 2015; Cuppen et al. 2017; Öberg & Bergin 2021). This leads to the formation of saturated molecules such as H_2O, NH_3, and CH_4 which remain situated as ices on the surface.

In the cold (< 15 K) conditions of prestellar cores, even the most volatile species like CO can *freeze out* onto the dust grains, making them available for grain-surface chemistry through for example hydrogenation. Sequential hydrogenation of CO ice results in the formation of HCO, formaldehyde (H_2CO), and eventually CH_3OH (Watanabe & Kouchi 2002; Fuchs et al. 2009; Santos et al. 2022). Methanol is the simplest and most abundant *complex organic molecule* (Herbst & van Dishoeck 2009) and a poster child of grain-surface chemistry since gas-phase chemistry producing CH_3OH is highly ineffective at low-temperature conditions (e.g., Garrod et al. 2006; Geppert et al. 2006).

The chemistry on the surfaces does not stop at CH_3OH. Many more complex species have been observed toward hot cores (see Sect. 1.4.2) and many laboratory studies have been carried out to explain their formation on the surfaces of dust grains. Reactions between pre-products of CH_3OH, such as HCO and CH_2OH, can lead to even more complex species such as glycolaldehyde (CH_2OHCHO) and ethylene glycol ($(CH_2OH)_2$; Fedoseev et al. 2015), and possibly even result in molecules as big as glycerol (Fedoseev et al. 2017). Furthermore, also the formation of several 3-carbon alcohols such as n-propanol ($CH_3CH_2CH_2OH$) was witnessed in the laboratory (Qasim et al. 2019a). Moreover, Fedoseev et al. (2022) find formation of ketene (H_2CCO), acetaldehyde (CH_3CHO), and ethanol (C_2H_5OH) in cold conditions by depositing CO together with atomic C and H. For some species such as methyl formate (CH_3OCHO), the chemistry seems to depend also on UV irradiation (Chuang et al. 2017). Alternatively, some COMs may also form through thermally induced chemistry (Theulé et al. 2013).

Interestingly, recent laboratory studies suggest that CO and its hydrogenation may not be required for the formation of all COMs. For multiple oxygen-bearing COMs such as CH_3CHO, H_2CCO, C_2H_5OH, and vinyl alcohol (C_2H_3OH), recent laboratory studies suggest that acetylene (C_2H_2) could be the initial molecule rather than (pre-products of) CH_3OH (Chuang et al. 2020, 2021). These molecules could thus already be made prior to CO freeze-out in the translucent cloud phase, and could even lead to the formation n-propenol, isopropenol, and glycine (Qasim et al. 2019b; Ioppolo et al. 2021).

The importance of grain-surface chemistry for nitrogen-bearing COMs remains far less well understood. The OCN^- anion and NH_3 remain the most complex nitrogen-bearing species that are securely detected in the ices (Grim & Greenberg 1987; Schutte & Greenberg 1997; Boogert et al. 2015). Although laboratory studies suggest that in the presence of UV irradiation nitrogen-bearing COMs such as ethyl cyanide (C_2H_5CN) can form from a methyl cyanide (CH_3CN) ice mixed with H_2O (Bulak et al. 2021), it remains unknown if and how CH_3CN forms in interstellar ices.

1.2.2 Hot cores

As the envelope material (both gas and dust) moves toward the accreting protostar, the physical conditions change due to the increase in density, temperature, and UV field (e.g., Aikawa et al. 1999; Visser et al. 2009; Drozdovskaya et al. 2014). As the dust grains heat up to 20–30 K, volatile ice species such as CO, N_2, and CH_4 start sublimating from the ices toward the gas phase. Despite the lower residence time of atomic H on the surfaces of dust grains, which hampers hydrogenation of molecules, modeling studies suggest that elevated dust temperatures (> 20 K) may actually be beneficial for forming complex molecules since species can diffuse more easily through the ices (Garrod & Herbst 2006; Garrod 2013; Garrod et al. 2022).

When the temperature reaches about 100-300 K in the central *hot core* (or *hot corino* for low-mass protostars), the most strongly bound species such as H_2O and COMs fully sublimate into the gas phase. In theory, each molecule has its own binding energy and will therefore sublimate at a different temperature (e.g., Collings et al. 2004; Penteado et al. 2017; Cuppen et al. 2017; Minissale et al. 2022), creating an onion shell-like structure of molecules. For example, species like H_2CCO, CH_3OH, CH_3CHO are relatively "cold" COMs sublimating at temperatures of 70-100 K, whereas $(CH_2OH)_2$ and formamide (NH_2CHO) likely sublimate at much higher temperatures of > 200 K (e.g., Fedoseev et al. 2017). However the binding energies of molecules are also very dependent on the ice mixture (whether they are bound to a H_2O or CO dominated ice) and even on the type of grain surface (e.g., Tielens et al. 1991; Collings et al. 2004; Ferrero et al. 2020) Furthermore, several studies also suggest that the majority of the COMs sublimate together with major ice species such as H_2O and CH_3OH at ~ 100 K.

The higher temperatures in hot cores also allow for endothermic reactions to occur more efficiently. Whilst several COMs such as CH_3OH do not have efficient gas-phase formation routes even at temperatures of > 100 K, some COMs such as NH_2CHO and CH_2OHCHO may have additional gas-phase formation routes (e.g., Skouteris et al. 2017, 2018). Moreover, other recent studies link the formation of primarily nitrogen-bearing COMs such as CH_3CN and C_2H_5CN to the $T > 300$ K region where these molecules are produced through top-down chemistry starting from sublimated carbon grains (van 't Hoff et al. 2020a). The most direct way to distinguish gas-phase chemistry from grain-surface chemistry is by comparing abundances in the ices (Sect. 1.4.1) with those observed in the gas (Sect. 1.4.2).

1.2.3 Shocks

Shocks are regions in space where the temperature and density increase significantly over a short distance and timescale through the collision of one "fluid" with another (see e.g., review by Draine & McKee 1993). They are common phenomena in the universe and can occur on large scales such as in supernova explosions as well as on smaller scales in for example late-type AGB stars. In young protostellar systems, shocks are often observed in the bipolar outflows and jets where the outflowing material impacts the surrounding envelope (e.g., McCaughrean et al. 1994) as well as internally within the jet (e.g, Lee et al. 2017a; Tychoniec et al. 2019).

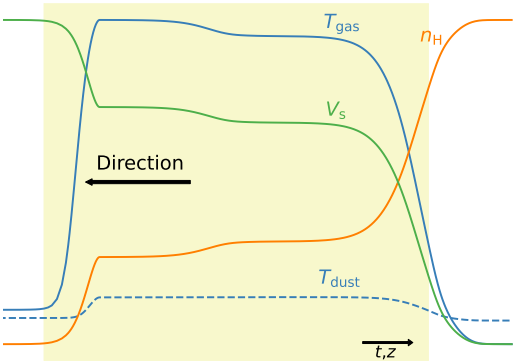

Figure 1.3: Schematic of the structure of a J-type shock. The hydrogen density and velocity are depicted in orange and green, respectively. The temperatures of the gas (solid) and dust (dashed) are shown in blue. The yellow shaded area indicates the shocked region. The black arrow denotes the direction in which the shock front propagates.

Another example of shocks in protostellar systems are those occurring where material is accreted onto the protostar itself (see e.g., review by Hartmann et al. 2016), which can be observed in less extincted sources in highly ionized species. On the disk scales of interest for this thesis, shocks are of significant importance in protostellar evolution at the disk-envelope interface (see Sect. 1.5). In this Section, first a short review of the physics of shocks is given before going into the shock chemistry.

Physics of interstellar shocks

Whenever a shock wave approaches at a velocity larger than the speed of sound, the material ahead has no warning about the approaching shock wave. As the shock wave hits, the material is compressed leading to a sudden, discrete, and irreversible increase in both temperature and density (see Fig. 1.3). In this compression, physical quantities such as mass, momentum, and energy are assumed to be conserved, allowing to write down a set of equations that govern the physics at the shock front (so-called Rankine-Hugoniot equations). These equations are commonly used to model the shock physics of interstellar shocks in a large variety of conditions (e.g., Flower & Pineau des Forêts 2003; Lesaffre et al. 2013; Godard et al. 2019).

The increase in temperature and density in the shock depends mainly on a few physical quantities: pre-shock density of hydrogen $n_{\rm H} = n({\rm H}) + 2n({\rm H_2})$, shock velocity $V_{\rm s}$, and magnetic field strength B. In the absence of a magnetic field, the pre-shock material has no knowledge at all about the approaching shock wave and therefore both the temperature and density jump up discontinuously, creating a so-called J-type shock. For J-type shocks, all the material (ions and neutrals) are tied to one fluid and the maximum gas temperature (in K) reached in the shock can be calculated through (Lesaffre et al. 2013),

$$T_{\rm gas,max} \approx 53 V_{\rm s}^2, \tag{1.3}$$

with $V_{\rm s}$ is the shock velocity in km s^{-1}. Similarly, the density can easily jump by more than 2 or 3 orders of magnitude in the post-shock region. The temperature of the dust ($T_{\rm dust}$), however, only increases at high pre-shock densities ($\gtrsim 10^7$ cm^{-3})

due to gas-grain collisions and never reaches as high temperatures as the gas. *J*-type shocks can drastically change the composition of the material as it enables effective high-temperature gas-phase chemistry, and for the highest velocities can lead to complete dissociation of all the molecules ($V_\mathrm{s} \gtrsim 25$ km s^{-1}; Flower & Pineau des Forêts 2003) and even ionize them ($V_\mathrm{s} \gtrsim 35$ km s^{-1}; Lehmann et al. 2020).

In the presence of a magnetic field, the material has a way of knowing that a shock front is coming. The sudden jump at the shock front becomes smoother when the shock velocity V_s is smaller than the magnetosonic speed of the ions,

$$c_\mathrm{ims} = \sqrt{c_\mathrm{i}^2 + B^2/4\pi\rho_\mathrm{i}^2}, \tag{1.4}$$

with c_i and ρ_i sound speed and density of the ions, respectively. When $V_\mathrm{s} < c_\mathrm{ims}$, a so-called magnetic precursor can develop: a region in front of the shock where the ions and electrons can decouple from the neutral species through the Lorentz force. Whilst slowing down, the ions exert a drag force on the neutral fluid, which therefore also smoothly decreases in velocity. The results is that ions, neutrals, and electrons decouple from each other, resulting in a continuous increase in both the temperature and the density (Draine 1980; Flower & Pineau des Forêts 2003). The resulting shock is referred to as a *C*-type shock. In intermediate magnetized environments, the drag force of the ions is insufficient to completely slow the neutrals before hitting the shock front and a discontinuous jump in density and temperature may still occur, creating a so-called *CJ*-type shock (Godard et al. 2019).

After the initial heating and compression, the shocked material starts to cool down. Depending on the heat released in the shock, cooling can be dominated by rotational and rovibrational transitions of simple molecules such as H_2, CO, and NH_3, or by optical and UV lines from atoms and ions (i.e., [OI], [SII]). Alternatively, gas-grain collisions in higher density shocks can contribute significantly to the cooling, where the gas transfers the heat to the dust which emits it away as thermal emission. Eventually, the shock cools down completely, leaving the now post-shock material irreversibly changed.

Chemistry of interstellar shocks

The gas-phase chemistry in shocks is dominated by endothermic reactions due to the high temperatures that are easily reached. A key reaction for shock chemistry is the formation of the highly reactive OH radical through,

$$\mathrm{O} + \mathrm{H_2} \rightarrow \mathrm{OH} + \mathrm{H}, \tag{1.5}$$

which has an energy barrier and starts to become efficient as temperatures reach > 100 K (see also Fig. 1.4). The OH radical is a very reactive molecule and therefore easily reacts with other molecules. At higher temperatures of > 300 K, the OH radical can react further with H_2 to from H_2O. Water is therefore a very important shock tracer in observations and is indeed commonly observed in high-velocity jets and outflows (e.g., with *Herschel*; Nisini et al. 2010; Herczeg et al. 2012; Kristensen et al. 2012; van Dishoeck et al. 2021).

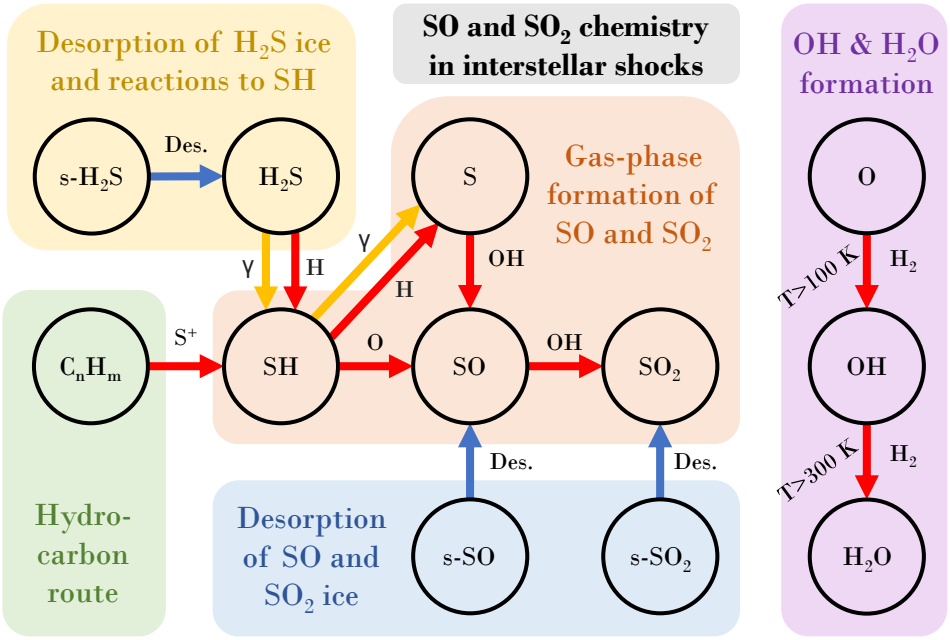

Figure 1.4: Diagram of the chemistry of SO and SO_2 in shocks. Only forward reactions are shown, with red arrows denoting gas-phase reactions, yellow arrows photodissociation reactions, and blue arrows ice desorption. The shaded colored regions highlighted various formation pathways.

Likewise, sulfur-bearing molecules such as SO and SO_2 are characteristic tracers of interstellar shocks. Similarly to H_2O, they form through sequential reactions of atomic S with OH radicals (see also Fig. 1.4),

$$S + OH \rightarrow SO + H, \tag{1.6}$$

$$SO + OH \rightarrow SO_2 + H. \tag{1.7}$$

Both these reactions occur very efficiently in high-temperature (> 100 K) shock conditions (Prasad & Huntress 1980; Hartquist et al. 1980). However, a main limitation is that at temperatures of > 300 K, all of the OH molecules will be consumed by H_2 to form H_2O, leaving little SO and SO_2 formation. This makes SO and SO_2 powerful tracers of shocks with temperatures between $100 \lesssim T_{\rm gas} \lesssim 300$ K. An alternative mechanism to form SO is through reactions between SH and atomic O (Hartquist et al. 1980), but little atomic O will be available once temperatures reach $> 100 - 300$ K. Moreover, one needs to form SH first through either reactions between hydrocarbons such as H_2CO with ionized sulfur (S^+), or alternatively through photodissociation of H_2S which requires the presence of a strong UV field. Another route to get gaseous SO and SO_2 in shocks is by thermal sublimation of sulfur-bearing ices in, for example, high-density accretion shocks (Miura et al. 2017). Both SO and SO_2 are therefore suggested to be good tracers of less energetic and high-density shocks such as those at the boundary between

the envelope and the disk (e.g., Sakai et al. 2014; Artur de la Villarmois et al. 2019, see Sect. 1.5).

Alternatively, there are also molecules in shocks which can solely form through interactions with dust grains. One key molecule tracing such interactions in shocks is SiO, which forms through the reaction of atomic Si with OH. In protostellar envelopes, almost all of the Si is locked up in refractory dust grains and is therefore not available for the chemistry. However, in *C*-type shocks, the Si can be sputtered of the dust grains through collisions between the gas and dust (Gusdorf et al. 2008a,b). Furthermore, in high-velocity *J*-type shocks, the dust grains may be thermally sputtered through collisions with heavy molecules or even completely sublimated (Guillet et al. 2009), therefore releasing Si back into the gas phase. Molecules like SiO are therefore powerful tracers of shocks such as those in high-velocity jets (e.g., Guilloteau et al. 1992; Tychoniec et al. 2019).

Also the ice mantle of dust grains can be sputtered. For ice sputtering to happen, it is crucial that the shock is of *C*-type since the drag between ions and neutrals allows for collisions of molecules with the dust grains. Through this process, dominant ice species like H_2O, CH_3OH, and other COMs can be released into the gas phase (e.g., Tielens et al. 1994; Arce et al. 2008; Suutarinen et al. 2014; Tychoniec et al. 2021).

1.3 Astronomical observatories

The largest advances in astronomical research are made when new observatories come online. These new observatories generally have significantly higher spatial and/or spectral resolution and sensitivity than their predecessors, resulting in exciting and often even unexpected results. In this Section, two observatories of particular importance for this thesis are discussed: ALMA and the *James Webb* Space Telescope (JWST).

1.3.1 ALMA

ALMA is an interferometer of in total 66 antennas that are situated at an altitude of 5000 m on the Chajnantor plateau of the Chilean Andes. The main array consists of 50 antennas with a diameter of 12 m that can be moved to different positions on the plateau. ALMA in its most compact configuration has maximum baselines of $\sim$ 150 m, corresponding to an angular resolution of $1.47''$ at a frequency of 230 GHz (1.3 mm). In its most extended configuration, the maximum baselines reach up to $\sim$ 16 km ($0.018''$ at 230 GHz). Besides the main array, also the Atacama Compact Array (ACA) consisting of 12 antennas with a diameter of 7 m and the Total Power array (four 12-m antennas) are situated on the Chajnantor plateau. The ACA is always fixed in the same configuration with a maximum baselines of 45 m ($5.45''$ at 230 GHz).

ALMA currently operates with 8 different receiver bands that can cover frequencies between 84 GHz (3.6 mm) and 950 GHz (0.32 mm) in between the strong atmospheric absorption bands. The total bandwidth that ALMA can observe

depends on the adopted spectral resolution (3.8 kHz − 15.6 MHz) but can not exceed 8 GHz. ALMA is therefore very suitable for observing rotational transitions of molecules. Furthermore, at millimeter wavelengths, the dust become (largely) optically thin, allowing for observing the dust continuum as well as molecular transitions deep within star-forming systems, for example in hot cores and protoplanetary disks.

The strong advantage of ALMA is the much higher angular resolution compared with single dish telescopes. Moreover, ALMA has unprecedented high sensitivity due to the high number of antennas, allowing for the detection of minor isotopologues (e.g., $^{13}C^{18}O$, $CH_3^{18}OH$). This is crucial for very abundant species for which spectral lines originating from the main isotopologue are optically thick; observing the optically thin isotopologues is then the only way to probe the total column of the main isotopologue. Furthermore, the high spectral resolution is important for molecular line studies of quiescent gas in, for example, protostellar envelopes since the spectral lines can be resolved down to ~ 0.01 km s^{-1}. However, one of the disadvantages of using interferometric observations is that large-scale emission is filtered out, therefore not allowing to map both small scales (i.e., disks) and larger scales (envelopes) in a single configuration. Fortunately, the ACA has large maximum resolvable scales (up to) $29''$ at 230 GHz, and with the Total Power array even the largest scales can be probed. Another disadvantage is the relatively small bandwidth that can be covered with ALMA. Several other interferometers, such as the Submillimeter Array (SMA) and the Northern Extended Millimeter Array (NOEMA), have recently been updated with new receivers allowing higher frequency coverage within a single observation. Moreover, both the SMA and NOEMA are situated on the northern hemisphere and therefore more suitable to observe star-forming regions with higher declination such as Perseus.

1.3.2 JWST

With the first images of JWST released on July 12 2022, the infrared sky between 0.6 μm and 28 μm has been reopened, see Fig. 1.5. To observe this wavelength region, it is crucial to go into space since molecules in the Earth's atmosphere such as O_2, H_2O and CO_2 block most key wavelength bands (Smette et al. 2015, see Fig. 1.6). Moreover, the Earth's atmosphere starts to thermally emit at wavelengths of $\gtrsim 2$ μm. This significantly hampers ground-based observations at infrared wavelengths and has therefore led to several earlier space missions such as the *Infrared Space Observatory* (ISO; Kessler et al. 1996) and the *Spitzer* Space Telescope (Werner et al. 2004).

The primary mirror of JWST has a diameter of 6.5 m, allowing for a spatial resolution between $\sim 0.07''$ at 0.6 μm to $\sim 2''$ at 28 μm. The Near Infrared Spectrograph (NIRSpec) and Mid-Infrared Instrument (MIRI) instruments of JWST can achieve a medium spectral resolving power up to $R = \Delta\lambda/\lambda \sim 3500$ at smaller wavelengths ($\lesssim 10$ μm) which drops to $R \sim 1000$ at the highest wavelengths. This is higher than *Spitzer* but unfortunately not as high as for example *Herschel* achieved at longer wavelengths ($\sim 60 - 660$ μm) and will not allow for spectrally resolved lines in protostellar systems, but comparison with high-spectral resolution

Figure 1.5: A multi-color image of the Carina Nebula as observed with the NIRCAM instrument of JWST. The colors represent the various filters used: F090W (blue), F187N (cyan), F200W (green), F470N (yellow), F335M (orange), and F444W (red). The image shows various substructures within the cloud with exceptional detail and proves the high potential of the science which will be done with JWST over the coming years. Figure credit: NASA, ESA, CSA, and STScI.

data from ALMA can still provide information on the kinematics. Where JWST also exceeds its predecessors significantly is the sensitivity, which is up to two orders of magnitude higher than *Spitzer* achieved. This allows for deep observations at high spatial resolution in significantly lower integration times.

JWST will be very powerful in tracing the hot gas in protostellar systems, for example originating from the warm disk surface layers or from shocks, through observations of rovibrational lines of molecules as well as atomic lines. Furthermore, several bands of polycyclic aromatic hydrocarbons (PAHs) are within the NIRSpec and MIRI wavelength ranges. Moreover, JWST will be able to observe ice absorption bands and more accurately constrain the ice composition in protostellar envelopes (see Sect. 1.4.1).

1.4 Complex organic molecules in protostellar systems

As discussed in Sect. 1.2.1 and argued in this thesis, the majority of the COMs likely form in the ices in the cold prestellar phases. As the ice coated dust grains move closer toward the protostar, the ices sublimate into the gas phase in the hot core (Sect. 1.2.2). There are two direct ways to observe COMs in young protostellar

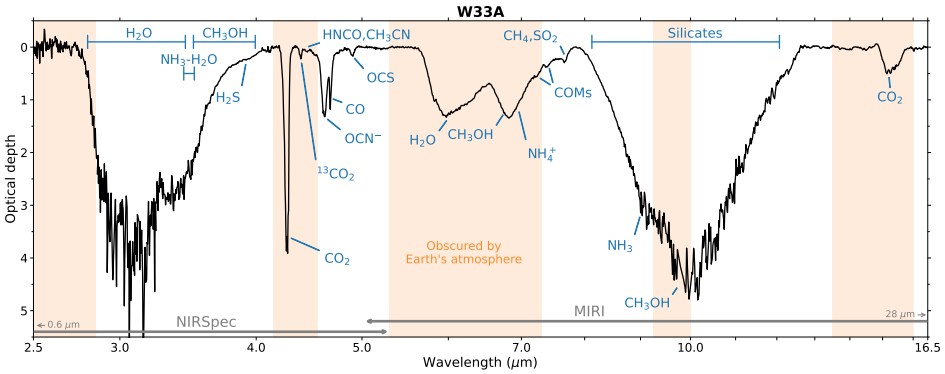

Figure 1.6: Infrared ice absorption spectrum taken with ISO toward the high-mass protostar W33A (Gibb et al. 2000). Various ice features are annotated together with their (presumed) molecular origin. In orange, the wavelength ranges that are completely obscured by the Earth's atmosphere are highlighted. At the bottom, the wavelength ranges of the NIRSpec and MIRI instrument of the *James Webb* Space Telescope are shown.

systems: in the ices through infrared absorption bands (Sect. 1.4.1) and in the gas phase through rotational transitions at millimeter wavelengths (Sect. 1.4.2).

1.4.1 Ices

Molecules that are frozen out onto dust grains are unable to rotate since they are locked up in an ice matrix. Therefore, they cannot emit light through rotational emission lines, making them harder to observe than gaseous molecules. However, molecules in ices can still vibrate and therefore absorb light in their vibrational modes. For almost all molecules, these lie at infrared wavelengths between $\sim 3 - 60$ μm (see review by e.g., Boogert et al. 2015).

Due to the limited sensitivities of spectrometers on early space telescopes such as ISO and *Spitzer*, only major ice species could be securely detected, mostly toward infrared-bright high-mass protostars, see Fig. 1.6. Water is one of the major ices and readily observed in high abundance (e.g., Boogert et al. 2008). Using observations of H_2O in various bands, even crystallized and amorphous water ice can be distinguished (e.g., Smith et al. 1989; Boogert et al. 2008; Terada & Tokunaga 2012). Similarly, strong ice absorption features are detected for other major ice species such as CO, CO_2 and NH_3 (e.g., Lacy et al. 1998; Gerakines et al. 1999; Pontoppidan et al. 2003b). However, more minor ice species remain difficult to detect. Definitive detections could still be made for molecules such as OCN^-, OCS, and CH_4 (Palumbo et al. 1997; van Broekhuizen et al. 2005; Öberg et al. 2008), but other molecules likely present in ices such as SO_2 and salts (NH_4^+) remain only tentatively identified (e.g., Knacke et al. 1982; Schutte & Khanna 2003; Boogert et al. 1997).

For similar reasons as mentioned above, the detection of COMs in ices remains

difficult. So far, CH_3OH is the only securely identified COM in the ices (e.g., Dartois et al. 1999; Pontoppidan et al. 2003a, 2004) and shows similar abundances with respect to H_2O across multiple low-mass sources (e.g., within about an order of magnitude; Boogert et al. 2008; Bottinelli et al. 2010). However, some other COMs do show tentative detections. The 7.2 μm and 7.4 μm bands were attributed to CH_3CHO and C_2H_5OH (Schutte et al. 1999; Öberg et al. 2011), but these could not be securely confirmed due to the low spectral resolution and/or sensitivity of ISO-SWS and *Spitzer*. Moreover, they were only (tentatively) detected in one absorption band that could also be attributed to other molecules such formic acid (HCOOH).

JWST will allow for the determination of not only the major ice species but also more minor species due to its significantly higher spatial and spectral resolution and sensitivity than previous infrared space observatories. Clear detections of key molecules such as SO_2 and COMs like CH_3CHO and C_2H_5OH are expected. This is also largely possible due to the many laboratory studies that have been carried out in the past decade to measure the infrared absorption bands of the majority of COMs such as CH_3CHO, C_2H_5OH, and CH_3OCH_3 (Terwisscha van Scheltinga et al. 2018), CH_3OCHO (Terwisscha van Scheltinga et al. 2021), acetone (CH_3COCH_3; Rachid et al. 2020), and methylamine (CH_3NH_2; Rachid et al. 2021).

1.4.2 Gas phase

Molecular emission can be directly observed through rotational lines at millimeter wavelengths as well as through rovibrational emission lines at infrared wavelengths. Since this thesis only uses pure rotational transitions, analyzing rovibrational lines will not be discussed further in detail.

Millimeter emission spectroscopy

Through collisions with mostly H_2, molecules can be excited into higher rotational energy states. They can subsequently return to the ground state either through collisions or via radiative decay through the emission of photons. The latter is much more effective than the former in (outer) protostellar envelopes due to the low densities. Hence, once a molecule is excited through a collision, it will decay back to its ground state by emitting photons at frequencies that are specific for each transitions of each molecule. Linear molecules such as CO have only few linearly spaced rotational energy levels (indicated with quantum number J) whereas more asymmetric rotating molecules such as CH_3OH and other COMs have many more available energy levels (indicated with quantum numbers J, K_a, K_c).

When the physical conditions of the gas in which a molecule resides can be approximated to be in *local thermodynamic equilibrium* (LTE, i.e., when collisional excitation balances collisional and radiative de-excitation), the level populations of a molecule can be described by a single *excitation temperature* $T_{\rm ex}$ through the Boltzmann distribution,

$$\frac{n_{\rm u}}{n_{\rm l}} = \frac{g_{\rm u}}{g_{\rm l}} \exp^{-\Delta E/k_{\rm B}T_{\rm ex}}, \tag{1.8}$$

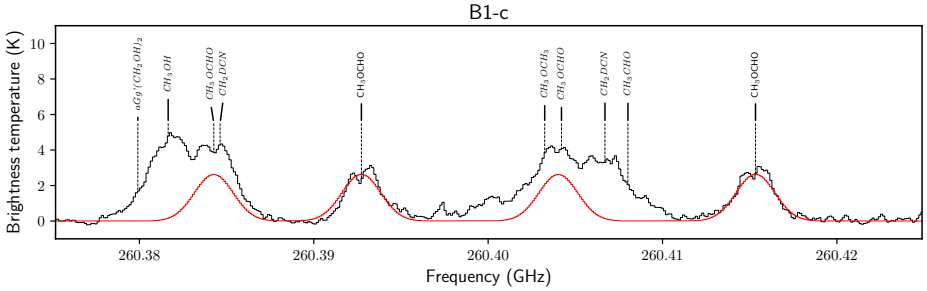

Figure 1.7: Part of the spectrum of the Class 0 protostar B1-c as observed with ALMA. The spectrum centered around four CH_3OCHO lines is shown in black with the best-fit model overplotted in red. The two blended transitions of CH_3OCHO are annotated in italics, as well as the species they are blended with. Based on fitting the other two unblended transitions of CH_3OCHO, the amount of emission of the blended lines that is originating from CH_3OCHO can be accurately estimated.

where n_u and n_l are the number densities of the upper (u) and lower (l) energy states, respectively, g_u and g_l their degeneracies, ΔE is the energy difference, and k_B the Boltzmann constant. It is important to note that in LTE conditions, the excitation temperature equals the physical gas temperature.

When one knows the relevant physical properties of the observed molecular transitions, such as the Einstein A_ul coefficients, upper energy level E_up, and partition function $Q(T_\mathrm{ex})$, one can construct a LTE model for a given T_ex to reproduce the observed line emission (for detailed description see e.g., Mangum & Shirley 2015). Through this method, the *column density* N of a molecule can be computed, which is the number of molecules per unit area observed within a solid angle Ω. If various transitions with a large range of E_up are covered, this also allows for an accurate determination of T_ex. Column densities are the direct observational quantity of the amount of a certain molecule; converting N (in cm^{-2}) to number density n (in cm^{-3}) is difficult since in astronomical observations the length of the column one measures is often difficult to constrain.

Several spectral analysis tools have been developed to analyze molecular emission lines. The tool primarily used in this work is CASSIS (Vastel et al. 2015), which uses the information on molecular transitions from both the Jet Propulsion Laboratory (JPL; Pickett et al. 1998) and the Cologne Database for Molecular Spectroscopy (CDMS; Müller et al. 2001, 2005; Endres et al. 2016). Note that the methods used in this thesis to derive the column densities and excitation temperatures are slightly different from the commonly used rotational diagrams (Goldsmith & Langer 1999). Instead of measuring each spectral line individually and combining them in such a rotational diagram, all spectral lines originating from a single molecule are included in a single calculation of N and T_ex, see Fig. 1.7. This is of particular importance in line-rich sources due to the severe line blending which can lead to over or underestimating the column densities from rotational diagrams.

Observations of hot cores

The central hot cores of young protostars have been studied extensively over the past decades. Before large interferometers such as SMA, NOEMA, and ALMA existed, the chemical content of these hot cores were observed with single dish telescopes and smaller interfometers such as the IRAM-30m telescope, James Clerk Maxwell Telescope (JCMT), and Caltech Owens Valley Radio Observatory (OVRO) or with space observatories such as the *Herschel* Space Observatory (e.g., Blake et al. 1987; van Dishoeck et al. 1995; Belloche et al. 2013; Crockett et al. 2015). However, the sensitivity of these single-dish studies is limited and the observations suffered from severe beam dilution, which hampers the detectability of compact hot cores. This is of particular relevance for detecting optically thin isotopologues which allow for much more stringent constraints on the molecular abundances. In this section, the focus is primarily on the recent results obtained mostly with interferometic observatories such as ALMA and NOEMA.

Initially, the COMs were mostly studied in detail in individual sources. Among the low-mass sources, the IRAS 16293-2422 (hereafter IRAS 16293) binary system is one of the best known hot cores and has been observed extensively over the past decades (van Dishoeck et al. 1995; Cazaux et al. 2003). The ALMA Protostellar Interferometric Line Survey (PILS; Jørgensen et al. 2016) targeted IRAS 16293 using the full bandwidth of the ALMA Band 7 receiver ($329 - 363$ GHz). The resulting spectra are extremely rich in spectral lines with about one line every 3 km s^{-1} (or 3.4 MHz, see Fig. 1.8). The PILS survey has led to several new molecular detections such deuterated formamide and acetic acid (NH_2CDO, NHDCHO, DNCO; Coutens et al. 2016), doubly deuterated methyl formate (CHD_2OCHO; Manigand et al. 2019), nitrous acid (HONO; Coutens et al. 2019), and chloromethane (CH_3Cl; Fayolle et al. 2017).

Among the high-mass sources, the Sagittarius B2 (hereafter Sgr B2) region and more nearby Orion KL regions are the best studied high-mass hot cores and are incredibly rich in their chemical content. Already in the pre-ALMA era, many first detections of COMs have been made toward these high-mass hot cores such as CH_3NH_2 (Kaifu et al. 1974), acetic acid (CH_3COOH; Mehringer et al. 1997), and CH_2OHCHO (Hollis et al. 2000). The chemical content of the Orion KL region was studied in depth with the OVRO spectral line survey, detecting 29 species in over 800 spectral lines (Blake et al. 1987). Similarly over 54 species in more than 4000 spectral lines were detected in a survey of Sgr B2(N) and Sgr B2(M) carried out with the IRAM 30m telescope (Belloche et al. 2013). More recently, with ALMA, the Sgr B2(N) region was resolved into several high-mass hot cores with narrower lines (Bonfand et al. 2017) and more stringent constraints on the chemical composition could be made (e.g., Belloche et al. 2014, 2016; Müller et al. 2016). Furthermore, with high-resolution ALMA data, the crowded region in Orion KL could be more easily disentangled allowing for more accurate studies of the hot core region (Pagani et al. 2017).

An interesting result from these single source studies is the physical differentiation between COMs within individual sources. With *Herschel*, significantly higher excitation temperatures were derived for nitrogen-bearing COMs ($200 - 300$ K)

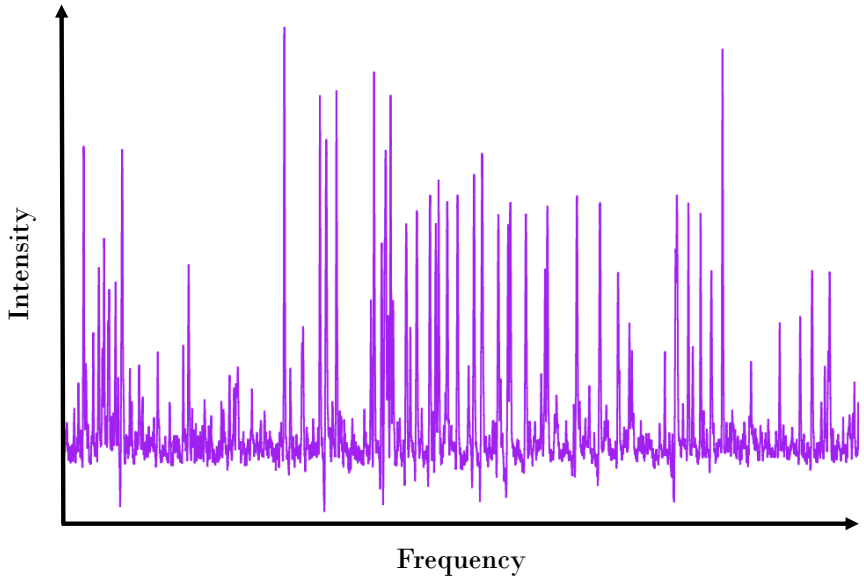

Figure 1.8: Part of the spectrum of the Class 0 protostar IRAS 16293-2422B as observed in the PILS survey at 338.5 GHz (Jørgensen et al. 2016). Only 1 GHz of bandwidth from the in total $\sim$ 33 GHz is shown. The y-axis ranges up to 0.8 Jy beam^{-1} and the noise level is at about 0.01 Jy beam^{-1}. Each peak is a spectral line originating from a rotational transitions of a molecule. Figure adopted from Jørgensen et al. (2016).

than for oxygen-bearing COMs in Orion KL which was attributed to a difference in sublimation temperature (Crockett et al. 2015). Similarly, varying excitation temperatures between $\sim 100 - 300$ K as well as different levels of deuteration (D/H $\sim 2 - 8$ %) were found for molecules in IRAS 16293B (Jørgensen et al. 2018). The former range was attributed to the COMs having different binding energies and thus sublimating at different temperatures. The latter range was suggested to originate from different formation times of the various COMs in the prestellar phases.

If indeed some COMs trace hotter regions closer to the protostar than others, the most straightforward way to verify this is to spatially resolve the hot core. Based on lower spatial resolution data with the SMA, Bisschop et al. (2008) suggested that there was spatial segregation between COMs toward IRAS 16293, but they could not yet spatially resolve individual hot cores. More recently, high-resolution ALMA data of a high-mass hot core show spatial segregation between nitrogen- and oxygen bearing COMs (Csengeri et al. 2019), but this difference likely originates from the oxygen-bearing COMs being released further out in either an accretion shock at the disk-envelope boundary or in the outflow rather than due passive heating by the protostar alone. Similarly, a physical differentiation between various COMs was observed in another high-mass hot core, but no clear link with the physical temperature structure in the source could be made (Law et al. 2021). For low-mass hot cores, only few high-resolution observations

are available, although these do show COMs emission originating, for example, from the surface of a disk (Lee et al. 2019a).

It is vital to compare various hot cores with each other in order to determine what physical or chemical properties set the chemical composition of young star-forming systems. Universal abundance ratios across various star-forming regions will point toward formation of COMs in similar physical conditions: on the surfaces of dust grains in cold prestellar cores. On the other hand, variations by orders of magnitude imply that local physical conditions such as temperature and UV field are crucial or that gas-phase chemistry in the hot cores can contribute. Some early single-dish observations suggested similar ratios of oxygen-bearing COMs with respect to CH_3OH but were affected by limited dynamical range (e.g., Jørgensen et al. 2005; Bergner et al. 2017). More recently, the CH_3OCHO/CH_3OCH_3 ratio was found to be remarkably constant (~ 1) across the full mass and evolutionary spectrum of protostellar evolution (Coletta et al. 2020), pointing toward very similar formation conditions between these two species. Also interferometric studies with ALMA en NOEMA show constant abundance ratios of several oxygen-bearing COMs with respect to CH_3OH (e.g., Jørgensen et al. 2018; Lee et al. 2019a; Jacobsen et al. 2019; Bergner et al. 2019; Bøgelund et al. 2019). However, differences between species become apparent as well, such as a bimodal abundance patterns between the isomers CH_3OCHO, CH_2OHCHO, and CH_3COOH in both low-mass and high-mass systems (El-Abd et al. 2019). Even protostars forming from the same cloud can show differences between their COMs abundances (e.g., IRAS 16293A and B; Manigand et al. 2020), although this could also be a physical effect (e.g., dust opacity; De Simone et al. 2020). Moreover, the deuteration of COMs such as CH_3OH seems to be significantly lower in high-mass protostars compared to their lower-mass counterparts (Bøgelund et al. 2018; Taquet et al. 2019), pointing toward higher temperatures in their prestellar phases. Nevertheless, these studies show that most COMs have comparable abundances across many star forming regions, suggesting similar formation conditions on the surfaces of dust grains in cold prestellar cores. Directly comparing the abundances in the gas phase with those to be derived in the ices with JWST for the same sources will further address this question.

Surprisingly, not all embedded protostars, high-mass or low-mass, show emission from COMs. Recent studies of larger samples of low-mass protostars have shown that only about $\sim 50-60\%$ show emission of CH_3OH originating from hot cores (Belloche et al. 2020; Yang et al. 2021), although the fraction of hot cores in some star forming regions can also be as low as $\sim 25\%$ (Bouvier et al. 2022). One reason for the absence of COMs emission from some sources could be low abundances of COMs in the ices, but this is not expected based on the large columns of CH_3OH ices that are observed toward protostellar envelopes (e.g., Pontoppidan et al. 2003a; Boogert et al. 2008; Bottinelli et al. 2010). A more likely explanation for the absence of COMs emission is the presence of a disk that affects the temperature structure in the system and casts a shadow on the envelope (Persson et al. 2016; Murillo et al. 2015, 2018, 2022). Alternatively, observations toward the protostellar binary system NGC 1333 IRAS 4A have shown that dust can become even optically thick at millimeter wavelengths and therefore hide the emission from

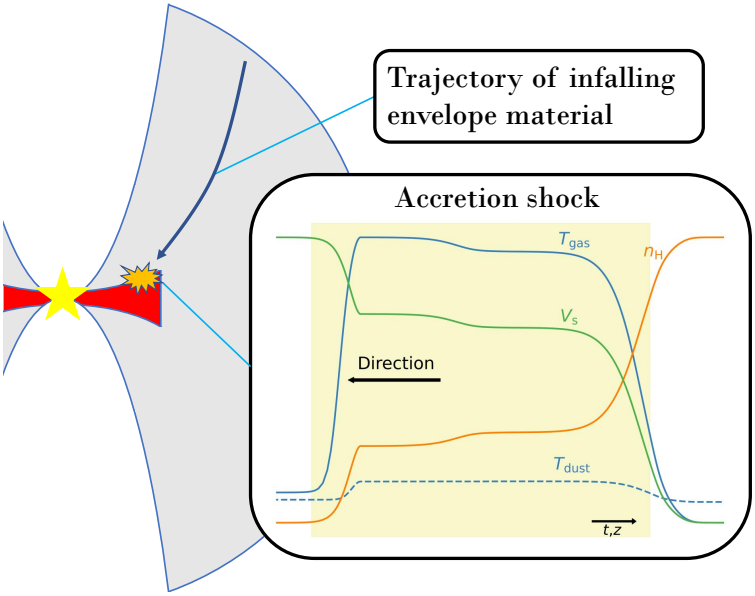

Figure 1.9: Simple schematic of a protostellar system highlighting the infall of envelope material onto the disk. At the disk-envelope boundary, an accretion shock may develop that can alter the chemistry.

the hot core (De Simone et al. 2020). Recent radiative transfer models have shown that both a disk and optically tick dust are needed to fully explain the absence of COMs emission in protostellar systems (Nazari et al. 2022b).

1.5 Inheritance versus reset: accretion shocks

Shocks are suggested to occur at the boundary between the infalling envelope and the surface of the disk, see Fig. 1.9. These shocks are commonly referred to as *accretion shocks*. The impact of such accretion shocks can be crucial for the evolution of the protostellar system. If the accretion shock is strong, it may (partially) *reset* the chemical composition (i.e., dissociate molecules into atoms) of the envelope material entering the disk. On the other hand, if the accretion shock is weak, it will not strongly affect the chemical composition and the hence the material entering the disk will be *inherited* from the parent envelope. Since planets are suggested to start forming in young embedded disks (Harsono et al. 2018; Tychoniec et al. 2020), the presence of an accretion shock is crucial for the composition of the material that is available for planet formation.

Numerical simulations of embedded protostellar systems frequently show accretion shocks (e.g., Cassen & Moosman 1981; Li et al. 2013). They can be very strong in the earliest phases when the disk is still small (< 1 au) and the velocities of infalling material high (> 10 km s^{-1}), leading to complete sublimation

or sputtering of the ices (Visser et al. 2009). This material, however, does not remain long in the disk and eventually ends up in the star, so it is not too relevant for the composition of a planet-forming disk. In later stages, when the disk is $\gtrsim$ 10 au, the strength of the accretion shock likely decreases due to lower infall velocities ($\lesssim$ 10 km s^{-1}) at larger radii, but the material entering the disk does not (directly) end up in the star. At these lower velocities, more strongly bound species such as H_2O likely remain in the ices (Visser et al. 2009; Miura et al. 2017). However, weaker bound species such as CO and SO can still be sublimated from the grain mantles. Moreover, the gas can reach temperatures of $>$ 1000 K (Neufeld & Hollenbach 1994), enabling high-temperature gas-phase chemistry.

Despite the predictions by models, accretion shocks have not yet been unambiguously detected. The cleanest and most direct tracers of high-velocity shocks are optical forbidden lines of atoms or ions such as [OI] 6300 Å and [SII] 6371 Å (e.g., Banzatti et al. 2019), but these are not viable for accretion shocks due to the severe extinction by the natal envelope. Alternative tracers are spectral lines at mid-infrared wavelengths such as the [SI] 25 μm, [OI] 63 μm, and rovibrational H_2O lines. However, current mid-infrared observatories lack the spatial resolution and sensitivity to resolve these lines in order to separate them from the outflow (e.g., Kristensen et al. 2012; Nisini et al. 2015). Fortunately, the launch of JWST will solve this problem. At submillimeter wavelengths, observations with ALMA have suggested that SO and SO_2 may be good tracers of accretion shocks. An enhancement of SO emission was observed at the disk-envelope boundary of a few embedded protostars that could be kinematically distinguished from the inner envelope (Sakai et al. 2014, 2017; Oya et al. 2019). Similarly, warm SO_2 emission showing rotational profiles are observed toward embedded protostars (Artur de la Villarmois et al. 2019; Bjerkeli et al. 2019). More recently, warm SO and SO_2 related to accretion shocks were even observed in more evolved Class II systems at the boundary between disk and accretion streamers (Garufi et al. 2022). However, warm SO and SO_2 are not unambiguous tracers of accretion shocks in protostellar systems as these species can also be present in outflows and jets (e.g., Lee et al. 2017a; Taquet et al. 2020), disk winds (e.g., Tabone et al. 2017, 2020; Lee et al. 2018), or in inner envelopes where they are passively heated by the central protostar (Harsono et al. 2021). It therefore remains difficult to interpret emission of SO and SO_2 related to accretion shocks. Comparison between observations and models is crucial to solve this ambiguity. Moreover, observations of mid-infrared shock tracers will more directly reveal the hot spots where accretion shocks are taking place.

Sophisticated shock models have been developed to derive the physical conditions of shocks. All shock models in this thesis are computed using the Paris-Durham shock code, which has been developed over the past decades (Flower et al. 1985; Flower & Pineau des Forêts 2003, 2015; Lesaffre et al. 2013; Godard et al. 2019). The Paris-Durham shock code computes the dynamical, thermal, and chemical structure of stationary plane parallel shock waves (see Sect. 1.2.3), taking into account important physical effects such as magnetic fields that can lead to the emergence of C, CJ, and J-type shocks. In the case of C and CJ-type shocks, up to three fluids (neutrals, ions, and electrons) can be included to properly model

the physical evolution. The thermal balance of both the gas and dust is consistently calculated throughout shock. Over 140 different species are included that can interact through $>$ 3000 chemical reactions. Moreover, an external UV field that irradiates the shock can be included that can be crucial for both the physical and chemical evolution of the shock by ionizing or dissociating molecules.

1.6 This thesis

This thesis aims to study how molecules are inherited from cloud to disk in young star-forming systems by studying both the physics and the chemistry. One of the main questions that is currently debated in the community is whether COMs form in the ices or in the gas phase. In order to answer this question two things are needed: 1) observations of gaseous COMs in much larger samples of hot cores than the handful of sources currently available and 2) direct detections of COMs in ices for the same sources. The focus of this thesis is on the gaseous content of oxygen-bearing COMs and on how universal gaseous COMs abundances are across multiple sources. This thesis also addresses whether the physical conditions in high-mass prestellar phases differ significantly from their lower-mass counterparts. Interestingly, some embedded sources do show emission originating from COMs while others do not. It remains uncertain whether this is a chemical effect (i.e., no COMs present at all) or a physical effect (i.e., COMs frozen out on dust grains or emission hidden by optically thick dust). Lastly, this thesis addresses the question of inheritance versus reset: is the chemical composition of planet-forming disks inherited from the cloud or is it (partially) reset in an accretion shock at the disk-envelope interface? The main results of this thesis are summarized below:

Chapter 2 presents observations with ALMA in Band 3 and Band 6 of several oxygen-bearing COMs in three low-mass protostars: B1-c, Serpens S68N, and B1-bS. The high spatial resolution and sensitivity of ALMA allowed for the detection of the optically thin $^{13}CH_3OH$ and $CH_3^{18}OH$ isotopologues which are crucial for the determination of abundance ratios with respect to CH_3OH. Using CASSIS, the column densities and excitation temperatures are derived. The abundance ratios of CH_3OCHO, CH_3OCH_3, CH_3COCH_3, and $(CH_2OH)_2$ with respect to CH_3OH are remarkably similar for the three studied sources, as well as when compared to other low-mass protostars studied with interferometric observations. Moreover, the three studies sources show similar deuteration ratios of methanol as other low-mass sources. On the other hand, the abundance ratios of C_2H_5OH, CH_3CHO, CH_2OHCHO, H_2CCO, and t-HCOOH with respect to CH_3OH show variations of more than an order of magnitude. Using the combined Band 3 and Band 6 data, a cold ($T_{\rm ex} < 70$ K) component of likely non-thermally desorbed COMs emission is found for B1-c with much lower column densities than the hot core.

Chapter 3 focuses on the emission of CH_3OH with the aim of determining why some embedded protostars do show emission of COMs and why others do not. A large sample of 148 low-mass and high-mass protostars is studied using ALMA data from Chapter 2, the Perseus ALMA Chemistry Survey (PEACHES), and the ALMA Evolutionary study of High Mass Protocluster Formation in the Galaxy

(ALMAGAL). Data for an additional 36 sources are added from the literature, giving a total of 184 different sources. Using the column density of CH_3OH derived from the optically thin ^{13}C and ^{18}O isotopologues, the warm ($T > 100$ K) gaseous methanol mass is derived for all sources and normalized by the dust mass derived from the dust continuum in order to take into account the mass of the inner envelope. A correlation between the normalized warm methanol mass and the bolometric luminosity $L_{\rm bol}$ was found, yet still a scatter of more than 4 orders of magnitude in the normalized warm methanol mass is present for both low-mass and high-mass sources. A simple toy model of a spherically symmetric infalling envelope provides a good fit to the sources with the highest normalized methanol mass. However, the large scatter can only be explained by the presence of (large) disks or by dust opacity effects, which is further investigated in Nazari et al. (2022b).

Chapter 4 studies the deuteration of methanol in high-mass protostars. Using the ALMAGAL data of Chapter 3, both singly (CH_2DOH) and doubly (CHD_2OH) deuterated methanol are used to derive the $(D/H)_{CH_3OH}$ and $(D/H)_{CH_2DOH}$ ratios for 98 high-mass protostellar systems. The observed $(D/H)_{CH_3OH}$ ratios of high-mass sources lie in the range of $10^{-3} - 10^{-2}$. Including also high-mass sources from the literature, the mean $(D/H)_{CH_3OH}$ is $1.3 \pm 0.8 \times 10^{-3}$, which is in good agreement with $(D/H)_{CH_3OH}$ derived for high-mass starless cores but more than an order of magnitude lower than $(D/H)_{CH_3OH}$ in low-mass protostars and low-mass prestellar cores. On the other hand, the average $(D/H)_{CH_2DOH}$ of high-mass sources is $2.0 \pm 0.7 \times 10^{-1}$, which is in good agreement with low-mass protostars. Based on a comparison between the observed $(D/H)_{CH_3OH}$ and GRAINOBLE models from the literature, we suggest that the high-mass prestellar phases are either warmer ($20-25$ K) than their lower mass counterpart (< 15 K) or, alternatively, high-mass prestellar phases have shorter timescales than low-mass prestellar phases.

Chapter 5 explores under which shock conditions the abundance of SO and SO_2 increases in accretion shocks at the disk-envelope interface. Detailed shock models of irradiated non-magnetized J-type shocks computed with the Paris-Durham shock code are presented for a large parameter space that is applicable for inner envelope conditions, that is, higher densities and lower shock velocities than for outflows. In low-velocity shocks (~ 3 km s^{-1}), the abundance of SO is increased through reactions of hydrocarbons (CH_4, H_2CO) with the S^+ anion and atomic O. At higher shock velocities (> 4 km s^{-1}), both SO and SO_2 are effectively formed as the shock cools down through subsequent reactions of atomic S with the OH radical. Here, the strength of the UV field is crucial through photodissociation of H_2O that formed earlier in the shock into OH. Thermal sublimation of SO and SO_2 ices only becomes relevant for higher densities ($\gtrsim 10^7$ cm^{-3}) and shock velocities (> 5 km s^{-1}).

Chapter 6 presents resolved ALMA observations with an angular resolution of $\sim 0.15''$(~ 10 au radius) of SO and SO_2 to search for the presence of accretion shocks in three Class I sources: TMC1A in Taurus and Ced 110 IRS 4 and IRS 6 in Chameleon. The dust disks in these three sources are clearly detected with radii of ~ 30 au, ~ 75 au, and ~ 50 au for TMC1A, IRS 4, and IRS 6, respec-

tively. Both SO and SO_2 are only detected toward TMC1A with narrow lines of 1.0 ± 0.1 km s^{-1}. An excitation temperature of 50 ± 20 K is derived for SO_2 and a SO_2/SO column density ratio of 0.6 ± 0.1. Based on the narrow lines, low excitation temperature, and comparison to sophisticated shock models, an accretion shock can be excluded as the origin of the SO and SO_2 emission. Similarly, the lack of SO and SO_2 toward the two Cederblad sources suggests the absence of a strong ($T_{\rm gas,max} > 100$ K) accretion shock. In turn, this implies that the chemical composition of these embedded disks could be directly inherited from their natal envelopes. Moreover, the presence of hot SO_2 originating from transitions with $E_{\rm up} > 100$ K seems to be correlated to the bolometric luminosity $L_{\rm bol}$, suggesting that energetic processes such as UV irradiation could be important for the chemistry of SO_2.

The main conclusions of this thesis are:

- Several oxygen-bearing COMs show remarkably similar abundance ratios with respect to CH_3OH between various low-mass protostars, indicating similar formation conditions, likely in the ices in the prestellar phases. On the other hand, the larger variation seen in some other COMs suggest that local physical conditions such as a UV field in an even earlier prestellar phase or gas-phase chemistry in the hot cores can contribute to their abundances.

- The absence of COMs emission in protostellar systems does not imply that they are not present. It rather shows that they are either still frozen out due to the presence of a disk or that their emission is hidden behind a layer of optically thick dust.

- High-mass prestellar phases are either warmer than their lower-mass counterpart or have shorter timescales.

- Warm SO and SO_2 emission can be used as a tracer of accretion shocks at the disk-envelope interface as long as a UV field is present.

The future of observations of both COMs in hot cores and accretion shocks is bright. ALMA has proven its worth with high resolution and sensitivity observations and will continue to provide us with new and exciting data. Where initially most ALMA studies focused on many COMs in single sources, the field is now shifting toward observing several COMs in a much larger sample of sources. This will give more insight on the chemical links between multiple COMs and their sensitivity to the physical conditions in the prestellar phases. Furthermore, more high-resolution ALMA observations of accretion shocks in SO, SO_2, but also other possible tracers such as H_2S and H_2CO will provide important information on the presence of such shocks and on their effect on the chemical composition.

With the launch of JWST, the mid-infrared sky will become available for astronomical observations at an unprecedented resolution and sensitivity. One of the key results that are expected are the detections of COMs larger than CH_3OH in the ices such as C_2H_5OH and CH_3CHO. Directly comparing the ice abundances to those derived in the gas phase for the same sources will be crucial for determining

the origin of COMs: ice chemistry of gas-phase chemistry. With JWST, also high-temperature infrared shock tracers such as [SI] 25 μm, rovibrational H_2O, and H_2 lines become available which can further constrain the presence and the strength of an accretion shock at the disk-envelope boundary and address the question of inheritance versus reset.